

Mixed GMsFEM for the simulation of waves in highly heterogeneous media

Eric T. Chung* and Wing Tat Leung†

September 20, 2021

Abstract

Numerical simulations of waves in highly heterogeneous media have important applications, but direct computations are prohibitively expensive. In this paper, we develop a new generalized multiscale finite element method with the aim of simulating waves at a much lower cost. Our method is based on a mixed Galerkin type method with carefully designed basis functions that can capture various scales in the solution. The basis functions are constructed based on some local snapshot spaces and local spectral problems defined on them. The spectral problems give a natural ordering of the basis functions in the snapshot space and allow systematic enrichment of basis functions. In addition, by using a staggered coarse mesh, our method is energy conserving and has block diagonal mass matrix, which are desirable properties for wave propagation. We will prove that our method has spectral convergence, and present numerical results to show the performance of the method.

1 Introduction

Numerical simulations of waves are important in many practical areas. For example, in computational seismology, accurate simulations of acoustic waves play a crucial role in determining subsurface properties [44, 43, 40, 34, 41, 35]. Traditionally, the wave equation can be numerically solved by finite difference methods, finite element methods, discontinuous Galerkin methods and spectral methods [17, 29, 39, 27, 36, 30, 32, 31, 37, 46, 47, 48, 6, 7]. In many applications, the media of interest are highly heterogeneous and contain many scales. The above methods require the use of very fine meshes to fully resolve the multiscale structure of the media. Though the numerical solutions to the wave equation have been shown to be accurate when the computational grid is fine enough [18], the practical limitations in discretization caused by limitations in computational power restrict this accuracy. It is therefore necessary to develop numerical approaches that can incorporate fine-scale features into coarse-grid based methods, where the coarse grid size is independent of the medium scales.

There are in literature some model reduction techniques aiming at solving the wave equation in media with multiple scales. For instances, in [5, 26, 24, 38, 33, 42], some numerical homogenization and upscaling based techniques are developed. In these methods, the heterogeneous medium is replaced by an effective medium which can be efficiently resolved by a coarse mesh, giving certain reduction in computational cost. In addition, various multiscale methods are developed in [14, 25, 1, 21, 23, 2, 22, 28], which also aim at discretizing the wave equation in a coarse grid by the use of the multiscale finite element method [20] or by the use of the heterogeneous multiscale method [45]. While the above are very successful methods, they can produce solutions with limited accuracy and sometimes fail to give correct solutions. Thus, there is a need to systematically enhance the accuracy within the model reduction framework. In this paper, we will focus on the recently developed Generalized Multiscale Finite Element Method (GMsFEM) [19]. The GMsFEM

*Department of Mathematics, The Chinese University of Hong Kong, Hong Kong SAR. This research is partially supported by the Hong Kong RGC General Research Fund (Project number: 400813).

†Department of Mathematics, Texas A&M University, College Station, TX.

is a generalization of the classical multiscale finite element method (MsFEM) [20] in the sense that multiple basis functions can be systematically added to each coarse element. The method consists of two stages: the offline stage and the online stage. In the offline stage, a space of locally supported snapshot functions is constructed. The snapshot space contains a large set of functions and can be used to capture essentially all fine-scale features of the solution. A space reduction is then performed by the use of a local spectral decomposition, and the dominant modes are taken as the multiscale basis functions. We notice that all these computations are done before the actual simulations of the solution. In the online stage, when a given source term or boundary condition is given, the above offline basis functions are used to obtain an approximate solution. One can also adaptively select the basis functions in various coarse elements in order to obtain better efficiency and accuracy [16, 15].

The purpose of this paper is to develop a new GMsFEM for the wave equation. There are previous works on GMsFEM for the wave equation based on the second order formulation and a discontinuous Galerkin framework [14, 25]. These methods give accurate simulations of waves in coarse meshes, but are lack of energy conservation. To develop a scheme with energy conservation, we consider the wave equation in the pressure-velocity formulation (called the mixed formulation). We will use some ideas from our earlier work on mixed GMsFEM for high contrast flows [13]. However, the method in [13] cannot be used directly for the wave equation since it is based on a piecewise constant approximation for pressure, which is not accurate for the wave equation, and the velocity basis functions give mass matrix that is not block diagonal. To derive a new GMsFEM with block diagonal mass matrix and energy conservation, we will use a staggered mesh [6, 7, 10, 11, 12, 8], where it is shown that such idea can give a numerical scheme with block diagonal mass matrix and energy conservation. In addition, this idea can give a smaller dispersion error [4, 9]. In [5, 26], we have applied a staggered coarse mesh in the numerical upscaling framework for the wave equation, where only one multiscale basis function is used for each coarse region. In this paper, we will develop a mixed GMsFEM based on a staggered mesh, giving block diagonal mass matrix, energy conservation and systematic enrichment of multiscale basis functions. In our new method, we will construct multiscale basis functions for both the pressure and the velocity. The construction follows the general methodology of GMsFEM by solving local spectral problems, which are carefully designed to achieve our goals. The spectral problems give a natural ordering of the basis functions according to the magnitudes of the corresponding eigenvalues. Dominant modes, those eigenfunctions with small eigenvalues, are taken as the basis functions and can be added systematically due to the natural ordering. Furthermore, we prove that the method is convergent, and the convergence rate is inversely proportional to the smallest eigenvalue of those eigenfunctions not selected in the basis set. Another advantage of using the mixed formulation is that perfectly matched layers can be used in conjunction with our method easily, and we will illustrate this in our numerical experiments.

The paper is organized as follows. In Section 2, we will state our problem and define some notations as well as the staggered mesh. In Section 3 and Section 4, we will give the constructions of our multiscale basis functions and our mixed GMsFEM. Section 5 is devoted to the convergence analysis of our method. In Section 6, we will present some numerical results to show the performance of our method. The paper ends with a Conclusion.

2 Problem description

Let $\Omega \subset \mathbb{R}^2$ be the computational domain. We consider the following wave equation in mixed formulation

$$\kappa \frac{\partial v}{\partial t} + \nabla p = 0 \quad \text{in } \Omega \quad (1)$$

$$\rho \frac{\partial p}{\partial t} + \nabla \cdot v = f \quad \text{in } \Omega \quad (2)$$

with homogeneous Dirichlet boundary condition $p = 0$ on $\partial\Omega$. We assume that the bulk modulus κ^{-1} and the density ρ are highly oscillatory. The aim of the paper is to construct multiscale basis functions, which provide accurate and efficient approximations of the pressure p and the velocity v on a coarse grid. The homogeneous Dirichlet boundary condition is chosen to simplify the discussions. Our method can be easily

applied to other types of boundary conditions as well as perfectly matched layers. Moreover, the extension of our method to the three dimensional case is straightforward.

First, we present the triangulation of the domain Ω . Let \mathcal{T}_0^H be an initial coarse triangulation of the domain. For each triangle in \mathcal{T}_0^H , we refine it into three triangles by connecting the centroid to the three vertices. The resulting refinement is called \mathcal{T}^H , which is our coarse mesh. Our multiscale basis functions are defined in this coarse mesh \mathcal{T}^H . We use \mathcal{E}_p to denote the set of all edges in the initial triangulation and use $\mathcal{E}_p^0 = \mathcal{E}_p \setminus \partial\Omega$. Moreover, we use \mathcal{E}_v to denote the set of new edges formed by the above division process. Note that, the set of all edges \mathcal{E}^H of the coarse mesh is $\mathcal{E}^H = \mathcal{E}_p \cup \mathcal{E}_v$, and the set of all interior edges $\mathcal{E}^{H,0}$ of the coarse mesh is $\mathcal{E}^{H,0} = \mathcal{E}_p^0 \cup \mathcal{E}_v$. The fine mesh \mathcal{T}^h is obtained by refining \mathcal{T}^H in the conforming way. We use \mathcal{E}^h to denote the set of edges in the fine mesh \mathcal{T}^h . An illustration of the above definitions is shown in Figure 1. In particular, the solid lines are the edges of the initial triangulation \mathcal{T}_0^H . By our construction, these lines also represent edges in \mathcal{E}_p . Moreover, the dash lines represent the new edges formed by the subdivision process. Note that, the coarse mesh \mathcal{T}^H is defined as the union of all the new triangles obtained from the subdivision process. We will discuss later the motivations and advantages of using such a mesh.

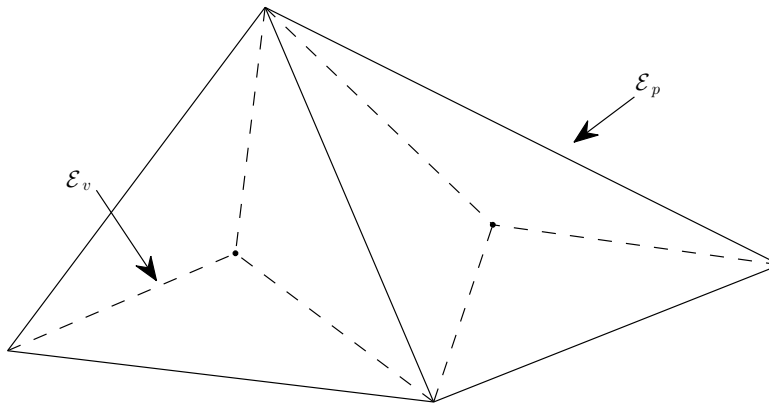


Figure 1: An illustration of the subdivision process and the definition of \mathcal{T}^H .

The wave equations (1)-(2) can be discretized on the fine mesh \mathcal{T}^h by the standard Raviart-Thomas finite element (RT0) method. Let (V_h, Q_h) be the standard RT0 space for (v, p) with respect to the fine mesh \mathcal{T}^h . Then, the RT0 method reads: find $v_h \in V_h$ and $p_h \in Q_h$ such that

$$\int_{\Omega} \kappa \frac{\partial v_h}{\partial t} \cdot w - \int_{\Omega} p_h \nabla \cdot w = 0, \quad \forall w \in V_h, \quad (3)$$

$$\int_{\Omega} \rho \frac{\partial p_h}{\partial t} q + \int_{\Omega} q \nabla \cdot v_h = \int_{\Omega} f q, \quad \forall q \in Q_h. \quad (4)$$

Notice that the RT0 scheme (3)-(4) does not have a block diagonal matrix. We will present a modified scheme for (1)-(2) based on the above RT0 method (3)-(4). The resulting method has the advantage that the mass matrix is block diagonal. We will use similar ideas as in [6, 7].

The main idea is to decouple the degrees of freedom for the velocity on the subset $\mathcal{E}^h \cap \mathcal{E}_p^0$ of fine grid edges, which are the fine grid edges lying in \mathcal{E}_p^0 . In particular, we do not enforce the continuity of the normal components of velocity on the fine grid edges in $\mathcal{E}^h \cap \mathcal{E}_p^0$. Moreover, we will introduce additional pressure variables in order to penalize the normal jumps of velocity on these edges.

We let \widehat{V}_h be the decoupled velocity space. That is, \widehat{V}_h is defined by using V_h and by decoupling the normal components of velocity on the fine grid edges in $\mathcal{E}^h \cap \mathcal{E}_p^0$. We will introduce an additional pressure

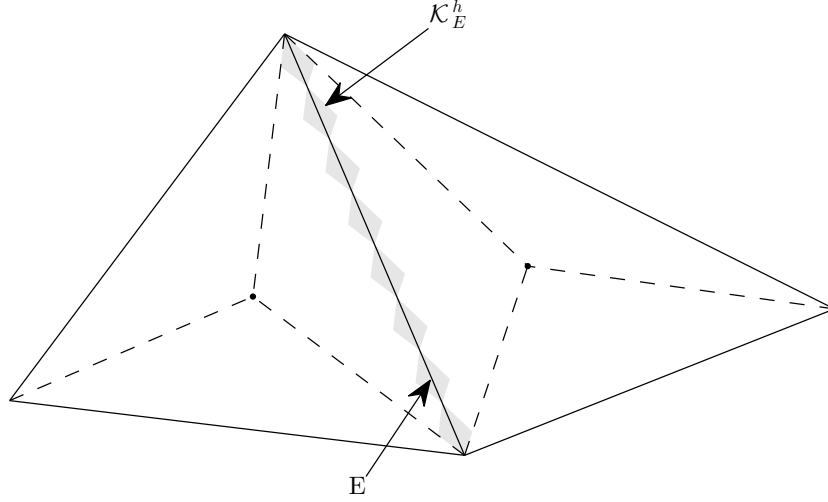


Figure 2: The definition of \mathcal{K}_E^h . The elements of \mathcal{K}_E^h are shown as shaded triangles.

space $\tilde{Q}_h \subset L^2(\Omega)$ as follows. Let $\mathcal{K}^h \subset \mathcal{T}^h$ be the set of fine mesh elements having non-empty intersection with \mathcal{E}_p . We also let $\mathcal{K}_E^h \subset \mathcal{K}^h$ be a subset containing fine mesh elements with non-empty intersection with $E \in \mathcal{E}_p$. See Figure 2 for an illustration. Then we define $q \in \tilde{Q}_h$ by the following conditions:

- $q|_\tau \in P^1(\tau)$ and $q|_e \in P^0(e)$, where $\tau \in \mathcal{K}^h$ and e is the edge of τ lying in \mathcal{E}_p ;
- $\int_\tau q = 0$ for all $\tau \in \mathcal{K}^h$;
- q is continuous on all edges $e \in \mathcal{E}^h \cap \mathcal{E}_p^0$.

Note that functions in \tilde{Q}_h have supports in \mathcal{K}^h . Then we define $\hat{Q}_h = Q_h + \tilde{Q}_h$. Note that we can impose the homogeneous Dirichlet boundary condition $p = 0$ in the space \tilde{Q}_h and we denote the resulting space by $\hat{Q}_{h,0}$. To construct $\hat{Q}_{h,0}$, we first define a subspace $\tilde{Q}_{h,0} \subset \tilde{Q}_h$ by $\tilde{Q}_{h,0} = \{q \in \tilde{Q}_h : q|_e = 0, \forall e \in \mathcal{E}_p \cap \partial\Omega\}$. Then we define $\hat{Q}_{h,0} = Q_h + \tilde{Q}_{h,0}$. We remark that the increase in the dimension by decoupling V_h to form \hat{V}_h is the same as the increase in the dimension by enriching the space Q_h to form \hat{Q}_h .

The modified numerical scheme is stated as follows. We find $v_h \in \hat{V}_h$ and $p_h \in \hat{Q}_{h,0}$ such that

$$\int_\Omega \kappa \frac{\partial v_h}{\partial t} \cdot w - \int_\Omega p_h^{(I)} \nabla \cdot w + \sum_{e \in \mathcal{E}^h \cap \mathcal{E}_p^0} \int_e p_h^{(B)} [w \cdot n] = 0, \quad \forall w \in \hat{V}_h, \quad (5)$$

$$\int_\Omega \rho \frac{\partial p_h}{\partial t} q + \int_\Omega q^{(I)} \nabla \cdot v_h - \sum_{e \in \mathcal{E}^h \cap \mathcal{E}_p^0} \int_e q^{(B)} [v_h \cdot n] = \int_\Omega f q, \quad \forall q \in \hat{Q}_{h,0}, \quad (6)$$

where $q^{(I)}$ and $q^{(B)}$ denote the components of q in the spaces Q_h and \tilde{Q}_h respectively, for any $q \in \hat{Q}_h$. The solution (v_h, p_h) of (5)-(6) is considered as the reference solution. In the following sections, we will construct multiscale solution (v_H, p_H) that gives good approximation of (v_h, p_h) and derive the corresponding error bound. Since the purpose of this paper is the construction and the analysis of a new multiscale method, the error analysis for the scheme (5)-(6) is not considered in this paper.

3 Multiscale basis functions

In this section, we will introduce multiscale basis functions and give the constructions of the multiscale approximation spaces V_H and Q_H for approximating v_h and p_h respectively. We emphasize that the basis functions and the corresponding multiscale method are defined with respect to the coarse mesh \mathcal{T}^H .

For a coarse element $K \in \mathcal{T}^H$, we define $V_h(K)$ as the restriction of V_h in K and $Q_h(K)$ as the restriction of Q_h in K . In addition, $V_{h,0}(K)$ is the subspace of $V_h(K)$ and contains vector fields whose normal components are zero on ∂K .

Below, we will give the definitions for the spaces Q_H and V_H . Our generalized multiscale finite element method reads: find $(v_H, p_H) \in V_H \times Q_H$ such that

$$\int_{\Omega} \kappa \frac{\partial v_H}{\partial t} \cdot w - \int_{\Omega} p_H \nabla \cdot w = 0, \quad \forall w \in V_H, \quad (7)$$

$$\int_{\Omega} \rho \frac{\partial p_H}{\partial t} q + \int_{\Omega} q \nabla \cdot v_H = \int_{\Omega} f q, \quad \forall q \in Q_H. \quad (8)$$

There are totally three set of basis functions. The first set of basis functions can be considered as a generalization of the RT0 element. The second set of basis functions gives enrichments of the normal component of velocity across coarse grid edges. The third set of basis functions corresponds to the standing modes within coarse elements with zero boundary conditions.

3.1 The first basis set

We use $V_H^{(1)}$ and $Q_H^{(1)}$ to denote the first set of basis functions for the velocity v and the pressure p . The space $Q_H^{(1)}$ is taken as the piecewise constant space with respect to the coarse mesh \mathcal{T}^H . We will define the space $V_H^{(1)}$ as follows. For each coarse edge $E \in \mathcal{E}^H$, we define ω_E as the union of all coarse elements having the edge E . For each $E \in \mathcal{E}^H$, we define one basis function $\phi_E^{(1)}$ whose support is ω_E . The basis $\phi_E^{(1)}$ is defined by finding $(\phi_E^{(1)}, p_E^{(1)}) \in V_h(K) \times Q_h(K)$ such that

$$\int_K \kappa \phi_E^{(1)} \cdot w - \int_K p_E^{(1)} \nabla \cdot w = 0, \quad \forall w \in V_{h,0}(K), \quad (9)$$

$$\int_K q \nabla \cdot \phi_E^{(1)} = \int_K c_E q, \quad \forall q \in Q_h(K) \quad (10)$$

for each $K \subset \omega_E$, with the following boundary condition

$$\phi_E^{(1)} \cdot n = \begin{cases} 1, & \text{on } E, \\ 0, & \text{on } \partial K \setminus E \end{cases} \quad (11)$$

where n denote the unit normal vectors on edges. In (10), the constant $c_E = |E|/|K|$. The space $V_H^{(1)}$ is defined by

$$V_H^{(1)} = \text{span} \left\{ \phi_E^{(1)} : E \in \mathcal{E}^H \right\}. \quad (12)$$

We remark that scheme (7)-(8) with $V_H = V_H^{(1)}$ and $Q_H = Q_H^{(1)}$ can be regarded as a generalization of the classical RT0 method.

3.2 The second basis set

We use $V_H^{(2)}$ to denote the second set of basis functions for the velocity v . We will see below that this corresponds to enrichments of velocity with respect to coarse grid edges. Notice that, in the second basis set, we only enrich the approximation space for the velocity. Let $E \in \mathcal{E}^H$. Note that $E \cap \mathcal{E}^h$ defines a

partition for E by fine grid edges. We define D_E be the space of piecewise constant functions on E with respect to the partition $E \cap \mathcal{E}^h$. Let \overline{D}_E be the subspace of D_E containing functions with zero mean. We write $\overline{D}_E = \text{span}\{\delta_{E,i} : i = 1, 2, \dots, N_E\}$, where N_E is the dimension of \overline{D}_E . For each $E \in \mathcal{E}^H$, we define a set of basis functions $\phi_{E,j}^{(2)}$ whose support is ω_E . We first find $(\psi_{E,i}^{(2)}, q_{E,i}^{(2)}) \in V_h(K) \times Q_h(K)$ such that

$$\int_K \kappa \psi_{E,i}^{(2)} \cdot w - \int_K q_{E,i}^{(2)} \nabla \cdot w = 0, \quad \forall w \in V_{h,0}(K), \quad (13)$$

$$\int_K q \nabla \cdot \psi_{E,i}^{(2)} = 0, \quad \forall q \in Q_h(K) \quad (14)$$

for each $K \subset \omega_E$, with the following boundary condition

$$\psi_{E,i}^{(2)} \cdot n = \begin{cases} \delta_{E,i}, & \text{on } E, \\ 0, & \text{on } \partial K \setminus E. \end{cases} \quad (15)$$

We next define a snapshot space $V_{E,\text{snap}}^{(2)}$ on E by

$$V_{E,\text{snap}}^{(2)} = \text{span}\{\psi_{E,i}^{(2)} : \forall \delta_{E,i} \in \overline{D}_E\}. \quad (16)$$

We remark that the snapshot space $V_{E,\text{snap}}^{(2)}$ is large and dimension reduction is necessary. To obtain a reduced dimension space, we use the following spectral problem. Find $\phi \in V_{E,\text{snap}}^{(2)}$ and $\lambda \in \mathbb{R}$ such that

$$\int_E (\phi \cdot n) (w \cdot n) = \lambda \int_{\omega_E} \kappa \phi \cdot w, \quad \forall w \in V_{E,\text{snap}}^{(2)}. \quad (17)$$

We arrange the eigenvalues in increasing order, that is, $\lambda_{E,1} < \lambda_{E,2} < \dots < \lambda_{E,N_E}$. For each coarse edge E , we take the first n_E eigenfunctions $\phi_{E,j}^{(2)}$. We then define

$$V_{E,\text{off}}^{(2)} = \text{span}\{\phi_{E,j}^{(2)} : j = 1, 2, \dots, n_E\}. \quad (18)$$

Finally, the space $V_H^{(2)}$ is defined as

$$V_H^{(2)} = \sum_{E \in \mathcal{E}^H} V_{E,\text{off}}^{(2)}. \quad (19)$$

3.3 The third basis set

We use $V_H^{(3)}$ and $Q_H^{(3)}$ to denote the third set of basis functions for the velocity v and the pressure p . We will see below that these basis functions correspond to some standing modes within coarse elements. Let $K \in \mathcal{T}^H$ be a given coarse element. We consider the following spectral problem: find $\psi \in V_{h,0}(K)$, $p \in Q_h(K)$ and $\mu \in \mathbb{R}$ such that

$$\int_K \kappa \psi \cdot w - \int_K p \nabla \cdot w = 0, \quad \forall w \in V_{h,0}(K), \quad (20)$$

$$\int_K q \nabla \cdot \psi = \mu \int_K \rho p q, \quad \forall q \in Q_h(K) \quad (21)$$

subject to the zero mean condition $\int_K p = 0$. Notice that the spaces $V_{h,0}(K)$ and $Q_h(K)$ are considered as the snapshot spaces. We arrange the eigenvalues in increasing order, that is, $\mu_{K,1} < \mu_{K,2} < \dots < \mu_{K,M_K}$, where $M_K + 1$ is the dimension of $Q_h(K)$. We will take the first m_K eigenfunctions $(\phi_{K,j}^{(3)}, p_{K,j}^{(3)})$ as basis. We define

$$V_{K,\text{off}}^{(3)} = \text{span}\{\phi_{K,j}^{(3)} : j = 1, 2, \dots, m_K\} \quad (22)$$

and

$$Q_{K,\text{off}}^{(3)} = \text{span}\{p_{K,j}^{(3)} : j = 1, 2, \dots, m_K\}. \quad (23)$$

Then we define

$$V_H^{(3)} = \sum_{K \in \mathcal{T}^H} V_{K,\text{off}}^{(3)} \quad \text{and} \quad Q_H^{(3)} = \sum_{K \in \mathcal{T}^H} Q_{K,\text{off}}^{(3)}. \quad (24)$$

Finally, we can take $V_H = V_H^{(1)} + V_H^{(2)} + V_H^{(3)}$ and $Q_H = Q_H^{(1)} + Q_H^{(3)}$ as the approximation spaces in the scheme (7)-(8).

4 The mixed GMsFEM

As discussed in the previous section, we can define the mixed GMsFEM for the wave equation by the system (7)-(8) together with the choices $V_H = V_H^{(1)} + V_H^{(2)} + V_H^{(3)}$ and $Q_H = Q_H^{(1)} + Q_H^{(3)}$ as the approximation spaces. However, the resulting scheme does not have a block diagonal mass matrix, and is therefore slow in the time stepping process. The reason for getting a non-diagonal mass matrix is that the basis functions in $V_H^{(1)}$ and $V_H^{(2)}$ have overlapping supports on two adjacent coarse elements. In particular, the basis functions for the velocity are coupled through the coarse grid edges \mathcal{E}^H . In the following, we will modify these spaces so that the velocity basis functions have disjoint supports. One important feature is that we will only decouple the basis functions on the coarse grid edges belonging to \mathcal{E}_p^0 only. We do not decouple the velocity basis functions for all coarse edges. The resulting velocity basis functions have disjoint supports on triangles of the initial coarse mesh \mathcal{T}_0^H , see Figure 1.

Let $E \in \mathcal{E}_p^0$ be a coarse edge. We recall that the basis functions in the space $V_H^{(1)}$ and $V_{E,\text{off}}^{(2)}$ have supports in ω_E and their normal components have common values on E . We will decouple this continuity, and call the resulting space as $\widehat{V}_H^{(1)}$ and $\widehat{V}_{E,\text{off}}^{(2)}$ respectively. In particular, the normal component of velocity does not necessarily have a single value on E . Globally, we define

$$\widehat{V}_H^{(2)} = \sum_{E \in \mathcal{E}^H} \widehat{V}_{E,\text{off}}^{(2)}. \quad (25)$$

We will introduce a new pressure space in order to penalize the normal continuity of velocity on $E \in \mathcal{E}_p^0$. Let $E \in \mathcal{E}_p$. This new pressure space is denoted by $Q_{E,\text{off}}^{(2)}$, and its dimension is $n_E + 1$. We recall that $\mathcal{K}_E^h \subset \mathcal{K}^h$ is the subset of fine elements having non-empty intersection with E , see Figure 2. The basis functions of $Q_{E,\text{off}}^{(2)}$ have supports on \mathcal{K}_E^h . Each $q \in Q_{E,\text{off}}^{(2)}$ is defined by the following conditions:

- $q|_\tau \in P^1(\tau)$ and $q|_e \in P^0(e)$, where $\tau \in \mathcal{K}_E^h$, and e is the edge of τ lying in E ;
- q is continuous on E , and $q = \phi \cdot n$ on E for some $\phi \in V_H^{(1)} \cup V_H^{(2)}$;
- $\int_\tau q = 0$ for all $\tau \in \mathcal{K}_E^h$.

We write

$$Q_{E,\text{off}}^{(2)} = \text{span}\{p_E^{(1)}\} + \text{span}\{p_{E,j}^{(2)} : j = 1, 2, \dots, n_E\}$$

where $p_E^{(1)} = 1$ on E and $p_{E,j}^{(2)} = \phi_{E,j}^{(2)} \cdot n$ on E . We define

$$\widehat{Q}_H^{(2)} = \sum_{E \in \mathcal{E}_p} Q_{E,\text{off}}^{(2)}. \quad (26)$$

Next, we discuss the boundary condition. We consider Dirichlet boundary condition $p = 0$ for pressure. We will need to modify the space $\widehat{Q}_H^{(2)}$ for the boundary condition. We define $\widehat{Q}_{H,0}^{(2)}$ by

$$\widehat{Q}_{H,0}^{(2)} = \sum_{E \in \mathcal{E}_p^0} Q_{E,\text{off}}^{(2)} \quad (27)$$

where the sum is taken over all interior edges $E \in \mathcal{E}_p^0$. We can take $V_H = \widehat{V}_H^{(1)} + \widehat{V}_H^{(2)} + V_H^{(3)}$ and $Q_H = Q_H^{(1)} + \widehat{Q}_{H,0}^{(2)} + Q_H^{(3)}$. Since the space V_H is not in $H(\text{div})$, we will replace the variational form (7)-(8) by the following. We find $(v_H, p_H) \in V_H \times Q_H$ such that

$$\int_{\Omega} \kappa \frac{\partial v_H}{\partial t} \cdot w - \int_{\Omega} p_H^{(I)} \nabla \cdot w + \sum_{E \in \mathcal{E}_p^0} \int_E p_H^{(B)} [w \cdot n] = 0, \quad \forall w \in V_H, \quad (28)$$

$$\int_{\Omega} \rho \frac{\partial p_H}{\partial t} q + \int_{\Omega} q^{(I)} \nabla \cdot v_H - \sum_{E \in \mathcal{E}_p^0} \int_E q^{(B)} [v_H \cdot n] = \int_{\Omega} f q, \quad \forall q \in Q_H \quad (29)$$

where we use $q^{(B)}$ to denote the component of q in $\widehat{Q}_{H,0}^{(2)}$ and $q^{(I)}$ to denote the component of q in $Q_H^{(1)} + Q_H^{(3)}$, for any $q \in Q_H$. Equations (28) and (29) give our mixed GMsFEM for the wave equation (1)-(2).

For the time discretization, we will apply the leap-frog scheme to (28)-(29). The velocity v_H are approximated at times $t_n = n\Delta t$, and the pressure p_H are approximated at times $t_{n+\frac{1}{2}} = (n + \frac{1}{2})\Delta t$, $n = 0, 1, \dots$.

We let v_H^n and $p_H^{n+\frac{1}{2}}$ be the approximate solutions at times t_n and $t_{n+\frac{1}{2}}$ respectively. The leap-frog scheme reads:

$$\int_{\Omega} \kappa \frac{v_H^{n+1} - v_H^n}{\Delta t} \cdot w - \int_{\Omega} p_H^{(I, n+\frac{1}{2})} \nabla \cdot w + \sum_{E \in \mathcal{E}_p^0} \int_E p_H^{(B, n+\frac{1}{2})} [w \cdot n] = 0, \quad \forall w \in V_H, \quad (30)$$

$$\int_{\Omega} \rho \frac{p_H^{n+\frac{3}{2}} - p_H^{n+\frac{1}{2}}}{\Delta t} q + \int_{\Omega} q^{(I)} \nabla \cdot v_H^{n+1} - \sum_{E \in \mathcal{E}_p^0} \int_E q^{(B)} [v_H^{n+1} \cdot n] = \int_{\Omega} f(t_{n+1}, \cdot) q, \quad \forall q \in Q_H \quad (31)$$

where $p_H^{(B, n+\frac{1}{2})}$ denotes the component of $p_H^{n+\frac{1}{2}}$ in $\widehat{Q}_{H,0}^{(2)}$ and $p_H^{(I, n+\frac{1}{2})}$ denotes the component of $p_H^{n+\frac{1}{2}}$ in $Q_H^{(1)} + Q_H^{(3)}$. We remark that the stability estimate for Δt can be obtained by standard techniques and the inverse estimate, see for example [26].

5 Theory

In this section, we will prove the stability and convergence of the mixed GMsFEM using the basis constructed in Section 4. We will also show that our method is energy conserving. To do these, we will first introduce some preliminary definitions which will be used in our analysis. Then, we will prove the energy conservation, stability and convergence for the mixed GMsFEM (28)-(29) with the use of $V_H = \widehat{V}_H^{(1)} + \widehat{V}_H^{(2)} + V_H^{(3)}$ and $Q_H = Q_H^{(1)} + \widehat{Q}_{H,0}^{(2)} + Q_H^{(3)}$ as the approximation spaces. We will assume zero initial values to simplify notations and analysis. We will also assume that the wave equation is solved from the initial time $t = 0$ to some finite time $t = T > 0$.

We define the inner product for the space \widehat{V}_h by

$$(v, w)_V = \int_{\Omega} \kappa v \cdot w$$

and the inner product for the space $\widehat{Q}_{h,0}$ by

$$(p, q)_Q = \int_{\Omega} \rho p q.$$

Then, the corresponding norms in the spaces \widehat{V}_h and $\widehat{Q}_{h,0}$ are induced by the inner products and are defined as

$$\|v\|_V^2 = (v, v)_V \quad \text{and} \quad \|p\|_Q^2 = (p, p)_Q. \quad (32)$$

Note that the above inner products and norms are also well-defined for V_H and Q_H since $V_H \subset \widehat{V}_h$ and $Q_H \subset \widehat{Q}_{h,0}$.

5.1 Energy conservation and stability

In this section, we will prove that the method (28)-(29) is energy conserving and is stable with respect to the norms (32). In particular, we will prove the following theorem.

Theorem 5.1. *Let $v_H \in V_H$ and $p_H \in Q_H$ be the solutions of (28)-(29). Then we have the following energy conservation property*

$$\frac{d}{dt} \frac{1}{2} (\|v_H\|_V^2 + \|p_H\|_Q^2) = 0 \quad (33)$$

provided $f = 0$. Moreover, the following stability holds

$$\max_{0 \leq t \leq T} (\|v_H(t, \cdot)\|_V^2 + \|p_H(t, \cdot)\|_Q^2) \leq 4 \left(\int_0^T \|\rho^{-1} f\|_Q \right)^2. \quad (34)$$

Proof. We take $w = v_H$ and $q = p_H$ in (28)-(29),

$$\int_{\Omega} \kappa \frac{\partial v_H}{\partial t} \cdot v_H + \int_{\Omega} \rho \frac{\partial p_H}{\partial t} p_H = \int_{\Omega} f p_H. \quad (35)$$

Thus, (33) holds when $f = 0$.

In addition, using (35) and the Cauchy-Schwarz inequality, we have

$$\frac{d}{dt} \frac{1}{2} (\|v_H\|_V^2 + \|p_H\|_Q^2) \leq \|\rho^{-1} f\|_Q \|p_H\|_Q. \quad (36)$$

Integrating in time from 0 to s ,

$$\|v_H(s, \cdot)\|_V^2 + \|p_H(s, \cdot)\|_Q^2 \leq 2 \int_0^s \|\rho^{-1} f\|_Q \|p_H(t, \cdot)\|_Q \leq 2 \max_{0 \leq t \leq T} \|p_H\|_Q \int_0^s \|\rho^{-1} f\|_Q.$$

So, we have

$$\max_{0 \leq t \leq T} (\|v_H(t, \cdot)\|_V^2 + \|p_H(t, \cdot)\|_Q^2) \leq 2 \max_{0 \leq t \leq T} \|p_H(t, \cdot)\|_Q \int_0^T \|\rho^{-1} f\|_Q.$$

Using the Cauchy-Schwarz inequality,

$$\max_{0 \leq t \leq T} (\|v_H(t, \cdot)\|_V^2 + \|p_H(t, \cdot)\|_Q^2) \leq \frac{1}{2} \max_{0 \leq t \leq T} \|p_H(t, \cdot)\|_Q^2 + 2 \left(\int_0^T \|\rho^{-1} f\|_Q \right)^2.$$

This implies (34). □

5.2 Convergence

In this section, we will prove the convergence of the mixed GMsFEM (28)-(29). Note that we can write $p_h^{(I)} \in Q_h$ in the following way

$$p_h^{(I)} = \sum_{K \in \mathcal{T}^H} \left(a_{K,0} + \sum_{j=1}^{M_K} a_{K,j} p_{K,j}^{(3)} \right) \quad (37)$$

where $a_{K,0}$ is the average value of $p_h^{(I)}$ on K , and $a_{K,j}$ are determined by

$$a_{K,j} = (p_h^{(I)}, p_{K,j}^{(3)})_Q, \quad j = 1, 2, \dots, M_K.$$

We remark that the dimension of $Q_h(K)$ is $M_K + 1$. In addition, we can write $p_h^{(B)} \in \tilde{Q}_{h,0}$ in the following way

$$p_h^{(B)} = \sum_{E \in \mathcal{E}_p^0} \left(b_{E,0} p_E^{(1)} + \sum_{j=1}^{N_E} b_{E,j} p_{E,j}^{(2)} \right) \quad (38)$$

where $b_{E,0}$ is the average value of $p_h^{(B)}$ on E , and $b_{E,j}$ are determined by

$$b_{E,j} = \int_E p_h^{(B)} \phi_{E,j}^{(2)} \cdot n, \quad j = 1, 2, \dots, N_E.$$

On the other hand, we can write $v_h \in \widehat{V}_h$ in the following way

$$v_h = \sum_{E \in \mathcal{E}^H} \left(c_{E,0} \phi_E^{(1)} + \sum_{j=1}^{N_E} c_{E,j} \phi_{E,j}^{(2)} \right) + \sum_{K \in \mathcal{T}^H} \sum_{j=1}^{M_K} d_{K,j} \phi_{K,j}^{(3)} \quad (39)$$

where $c_{E,0}$ is the average value of $v_h \cdot n$ on E , $c_{E,j}$ and $d_{K,j}$ are determined by

$$c_{E,j} = \int_E (v_h \cdot n) (\phi_{E,j}^{(2)} \cdot n), \quad j = 1, 2, \dots, N_E$$

and

$$d_{K,j} = \int_K \kappa v_h \cdot \phi_{K,j}^{(3)}, \quad j = 1, 2, \dots, M_K$$

respectively.

Using (37)-(39), we define the following interpolants $\pi(p_h^{(I)}) \in Q_H$, $\pi(p_h^{(B)}) \in Q_H$ and $\pi(v_h) \in V_H$ by

$$\begin{aligned} \pi(p_h^{(I)}) &= \sum_{K \in \mathcal{T}^H} \left(a_{K,0} + \sum_{j=1}^{m_K} a_{K,j} p_{K,j}^{(3)} \right), \\ \pi(p_h^{(B)}) &= \sum_{E \in \mathcal{E}_p^0} \left(b_{E,0} + \sum_{j=1}^{n_E} b_{E,j} p_{E,j}^{(2)} \right), \\ \pi(v_h) &= \sum_{E \in \mathcal{E}^H} \left(c_{E,0} \phi_E^{(1)} + \sum_{j=1}^{n_E} c_{E,j} \phi_{E,j}^{(2)} \right) + \sum_{K \in \mathcal{T}^H} \sum_{j=1}^{m_K} d_{K,j} \phi_{K,j}^{(3)}. \end{aligned} \quad (40)$$

Notice that in the above definitions of interpolants, we only sum over all basis functions in the spaces Q_H and V_H , instead of summing over all functions as in (37)-(39).

Next, we prove the following lemma concerning some properties of the interpolants defined in (40).

Lemma 5.2. *The interpolants $\pi(p_h^{(I)}) \in Q_H$, $\pi(p_h^{(B)}) \in Q_H$ and $\pi(v_h) \in V_H$ defined in (40) satisfy the following conditions*

$$\int_{\Omega} (p_h^{(I)} - \pi(p_h^{(I)})) \nabla \cdot w = 0 \quad (41)$$

$$\sum_{E \in \mathcal{E}_p^0} \int_E (p_h^{(B)} - \pi(p_h^{(B)})) [w \cdot n] = 0 \quad (42)$$

for all $w \in V_H$, and

$$\int_{\Omega} q^{(I)} \nabla \cdot (v_h - \pi(v_h)) = 0 \quad (43)$$

$$\sum_{E \in \mathcal{E}_p^0} \int_E q^{(B)} [(v_h - \pi(v_h)) \cdot n] = 0 \quad (44)$$

for all $q \in Q_H$.

Proof. By definition, we have

$$p_h^{(I)} - \pi(p_h^{(I)}) = \sum_{K \in \mathcal{T}^H} \left(\sum_{j=m_K+1}^{M_K} a_{K,j} p_{K,j}^{(3)} \right).$$

Taking $q = p_{K,j}^{(3)}$ in (10), we have

$$\int_K p_{K,j}^{(3)} \nabla \cdot \phi_E^{(1)} = \int_K c_E p_{K,j}^{(3)} = 0$$

since $p_{K,j}^{(3)}$ has zero mean on K . We see that (41) holds when $w \in V_H^{(1)}$. Now we take $q = p_{K,j}^{(3)}$ in (14) to get

$$\int_K p_{K,j}^{(3)} \nabla \cdot \phi_{E,i}^{(2)} = 0, \quad \forall i = 1, 2, \dots, n_E.$$

This shows that (41) holds when $w \in V_H^{(2)}$. Finally, using $q = p_{K,j}^{(3)}$ in (21), we have

$$\int_K p_{K,j}^{(3)} \nabla \cdot \phi_{E,i}^{(3)} = \int_K \rho r p_{K,j}^{(3)}, \quad \forall i = 1, 2, \dots, m_K$$

where $r = \text{span}\{p_{K,i}^{(3)} : i = 1, 2, \dots, m_K\}$. This shows that (41) holds when $w \in V_H^{(3)}$.

By definition, we have

$$p_h^{(B)} - \pi(p_h^{(B)}) = \sum_{E \in \mathcal{E}_p^0} \left(\sum_{j=n_E+1}^{N_E} b_{E,j} p_{E,j}^{(2)} \right).$$

It is clear that (42) holds when $w \in V_H^{(3)}$ since w vanishes on all coarse edges. It is also clear that (42) holds when $w \in V_H^{(1)}$ since $w \cdot n$ is a constant function on all coarse edges and $p_{E,j}^{(2)}$ has zero average on all coarse edges. By the spectral problem (17), $p_{E,j}^{(2)}$ is orthogonal to $w \cdot n$ on $E \in \mathcal{E}_p^0$ for all $w \in V_H^{(2)}$, so equation (42) holds when $w \in V_H^{(2)}$.

By definition, we have

$$v_h - \pi(v_h) = \sum_{E \in \mathcal{E}^H} \left(\sum_{j=n_E+1}^{N_E} c_{E,j} \phi_{E,j}^{(2)} \right) + \sum_{K \in \mathcal{T}^H} \sum_{j=m_K+1}^{M_K} d_{K,j} \phi_{K,j}^{(3)}.$$

The proofs for (43) and (44) are similar to the proofs of (41) and (42) and can be obtained by the same techniques above. \square

Now we prove the convergence. Subtracting (28)-(29) from (5)-(6),

$$\int_{\Omega} \kappa \frac{\partial(v_h - v_H)}{\partial t} \cdot w - \int_{\Omega} (p_h^{(I)} - p_H^{(I)}) \nabla \cdot w + \sum_{E \in \mathcal{E}_p^0} \int_E (p_h^{(B)} - p_H^{(B)}) [w \cdot n] = 0, \quad (45)$$

$$\int_{\Omega} \rho \frac{\partial(p_h - p_H)}{\partial t} q + \int_{\Omega} q^{(I)} \nabla \cdot (v_h - v_H) - \sum_{E \in \mathcal{E}_p^0} \int_E q^{(B)} [(v_h - v_H) \cdot n] = 0, \quad (46)$$

for all $w \in V_H$ and $q \in Q_H$. Using Lemma 5.2,

$$\int_{\Omega} \kappa \frac{\partial(v_h - v_H)}{\partial t} \cdot w - \int_{\Omega} (\pi(p_h^{(I)}) - p_H^{(I)}) \nabla \cdot w + \sum_{E \in \mathcal{E}_p^0} \int_E (\pi(p_h^{(B)}) - p_H^{(B)}) [w \cdot n] = 0, \quad (47)$$

$$\int_{\Omega} \rho \frac{\partial(p_h - p_H)}{\partial t} q + \int_{\Omega} q^{(I)} \nabla \cdot (\pi(v_h) - v_H) - \sum_{E \in \mathcal{E}_p^0} \int_E q^{(B)} [(\pi(v_h) - v_H) \cdot n] = 0, \quad (48)$$

for all $w \in V_H$ and $q \in Q_H$. Taking $w = \pi(v_h) - v_H$ and $q = \pi(p_h^{(I)}) - p_H^{(I)} + \pi(p_h^{(B)}) - p_H^{(B)}$, and adding the resulting equations, we have

$$\int_{\Omega} \kappa \frac{\partial(v_h - v_H)}{\partial t} \cdot (\pi(v_h) - v_H) + \int_{\Omega} \rho \frac{\partial(p_h - p_H)}{\partial t} (\pi(p_h^{(I)}) + \pi(p_h^{(B)}) - p_H) = 0. \quad (49)$$

Thus, we obtain

$$\begin{aligned} & \max_{0 \leq t \leq T} \left(\|\pi(v_h) - v_H\|_V + \|\pi(p_h^{(I)}) + \pi(p_h^{(B)}) - p_H\|_Q \right) \\ & \leq \int_0^T \left(\|\pi(\dot{v}_h) - \dot{v}_h\|_V + \|\pi(\dot{p}_h^{(I)}) + \pi(\dot{p}_h^{(B)}) - \dot{p}_h\|_Q \right) \end{aligned} \quad (50)$$

where the dots denote time derivatives. Hence, it suffices to estimate the interpolation errors.

In the following two theorems, we give error estimates of the interpolants. We remark that the notation $\alpha \lesssim \beta$ means that $\alpha \leq c\beta$ for some constant $c > 0$ independent of the mesh.

Theorem 5.3. *The interpolant $\pi(v_h)$ defined in (40) satisfies*

$$\|v_h - \pi(v_h)\|_V^2 \lesssim \left(\max_{E \in \mathcal{T}^H} \lambda_{E, n_E+1}^{-1} \right) \sum_{E \in \mathcal{E}^H} \int_E (v_h \cdot n)^2 + \left(\max_{K \in \mathcal{T}^H} \mu_{K, m_K+1}^{-1} \right) \|\rho^{-1} f - \dot{p}_h\|_Q^2. \quad (51)$$

Proof. By definition, we have

$$v_h - \pi(v_h) = \sum_{E \in \mathcal{E}^H} \left(\sum_{j=n_E+1}^{N_E} c_{E,j} \phi_{E,j}^{(2)} \right) + \sum_{K \in \mathcal{T}^H} \sum_{j=m_K+1}^{M_K} d_{K,j} \phi_{K,j}^{(3)} := z_1 + z_2.$$

By the orthogonality of eigenfunctions of the spectral problem (17),

$$\|z_1\|_V^2 \lesssim \sum_{E \in \mathcal{E}^H} \lambda_{E, n_E+1}^{-1} \int_E (v_h \cdot n)^2.$$

From (6), we have

$$\int_{\Omega} q \nabla \cdot v_h = \int_{\Omega} f q - \int_{\Omega} \rho \frac{\partial p_h}{\partial t} q \quad (52)$$

for all $q \in Q_H^{(3)}$. Using the fact that $\int_K q = 0$ for all $q \in Q_H^{(3)}$, we have

$$\int_{\Omega} q \nabla \cdot v_h = \sum_{K \in \mathcal{T}^H} \sum_{j=1}^{M_K} d_{K,j} \int_K q \nabla \cdot \phi_{K,j}^{(3)}.$$

By the spectral problem (21),

$$\int_{\Omega} q \nabla \cdot v_h = \sum_{K \in \mathcal{T}^H} \sum_{j=1}^{M_K} d_{K,j} \mu_{K,j} \int_K \rho p_{K,j}^{(3)} q.$$

Taking $q = p_{K,j}^{(3)}$, and using the condition that $\int_K \rho p_{K,i}^{(3)} p_{K,j}^{(3)} = \delta_{ij}$, we see that

$$d_{K,j} \mu_{K,j} = \int_{\Omega} p_{K,j}^{(3)} \nabla \cdot v_h, \quad j = 1, 2, \dots, M_K, \quad K \in \mathcal{T}^H. \quad (53)$$

Thus, by the spectral problem (20)-(21), we obtain

$$\|z_2\|_V^2 \lesssim \sum_{K \in \mathcal{T}^H} \sum_{j=m_K+1}^{M_K} d_{K,j}^2 (\phi_{K,j}^{(3)}, \phi_{K,j}^{(3)})_V = \sum_{K \in \mathcal{T}^H} \sum_{j=m_K+1}^{M_K} d_{K,j}^2 \mu_{K,j}.$$

Using (53) and then (52),

$$\|z_2\|_V^2 \lesssim \sum_{K \in \mathcal{T}^H} \sum_{j=m_K+1}^{M_K} \int_{\Omega} d_{K,j} p_{K,j}^{(3)} \nabla \cdot v_h = \int_{\Omega} \left(f - \rho \frac{\partial p_h}{\partial t} \right) \sum_{K \in \mathcal{T}^H} \sum_{j=m_K+1}^{M_K} d_{K,j} p_{K,j}^{(3)}.$$

Hence, we have

$$\|z_2\|_V^2 \lesssim \left(\max_{K \in \mathcal{T}^H} \mu_{K,m_K+1}^{-1} \right) \|\rho^{-1} f - \dot{p}_h\|_Q^2$$

since

$$\left\| \sum_{K \in \mathcal{T}^H} \sum_{j=m_K+1}^{M_K} d_{K,j} p_{K,j}^{(3)} \right\|_Q^2 \leq \left(\max_{K \in \mathcal{T}^H} \mu_{K,m_K+1}^{-1} \right) \|z_2\|_V^2$$

by the spectral problem (20)-(21).

This completes the proof of this theorem. \square

Theorem 5.4. *The interpolants $\pi(p_h^{(I)})$ and $\pi(p_h^{(B)})$ defined in (40) satisfy*

$$\|p_h^{(I)} - \pi(p_h^{(I)})\|_Q^2 \leq \left(\max_{K \in \mathcal{T}^H} \mu_{K,m_K+1}^{-1} \right) \|\dot{v}_h\|_V^2, \quad (54)$$

$$\|p_h^{(B)} - \pi(p_h^{(B)})\|_Q^2 \lesssim h \left(\max_{E \in \mathcal{E}_p^0} \lambda_{E,n_E+1}^{-1} \right) \|\dot{v}_h\|_V^2. \quad (55)$$

Proof. By the definition of $\pi(p_h^{(I)})$, we have

$$p_h^{(I)} - \pi(p_h^{(I)}) = \sum_{K \in \mathcal{T}^H} \left(\sum_{j=m_K+1}^{M_K} a_{K,j} p_{K,j}^{(3)} \right).$$

By the orthogonality of eigenfunctions $\{p_{K,j}^{(3)}\}$ and the spectral problem (21), we have

$$\|p_h^{(I)} - \pi(p_h^{(I)})\|_Q^2 = (p_h^{(I)} - \pi(p_h^{(I)}), p_h^{(I)})_Q = \int_{\Omega} p_h^{(I)} \nabla \cdot \left(\sum_{K \in \mathcal{T}^H} \sum_{j=m_K+1}^{M_K} a_{K,j} \mu_{K,j}^{-1} \phi_{K,j}^{(3)} \right).$$

We write $r_1 = \sum_{K \in \mathcal{T}^H} \sum_{j=m_K+1}^{M_K} a_{K,j} \mu_{K,j}^{-1} \phi_{K,j}^{(3)}$. Using (5), we have

$$\int_{\Omega} p_h^{(I)} \nabla \cdot r_1 = \int_{\Omega} \kappa \frac{\partial v_h}{\partial t} \cdot r_1 \leq \|\dot{v}_h\|_V \|r_1\|_V.$$

By the orthogonality of eigenfunctions $\{\phi_{K,j}^{(3)}\}$,

$$\|r_1\|_V^2 = \sum_{K \in \mathcal{T}^H} \sum_{j=m_K+1}^{M_K} (a_{K,j} \mu_{K,j}^{-1})^2 (\phi_{K,j}^{(3)}, \phi_{K,j}^{(3)})_V = \sum_{K \in \mathcal{T}^H} \sum_{j=m_K+1}^{M_K} (a_{K,j})^2 \mu_{K,j}^{-1} (p_{K,j}^{(3)}, p_{K,j}^{(3)})_Q$$

which implies

$$\|r_1\|_V^2 \leq \left(\max_{K \in \mathcal{T}^H} \mu_{K,m_K+1}^{-1} \right) \|p_h^{(I)} - \pi(p_h^{(I)})\|_Q^2.$$

This proves (54).

By the definition of $\pi(p_h^{(B)})$, we have

$$p_h^{(B)} - \pi(p_h^{(B)}) = \sum_{E \in \mathcal{E}_p^0} \left(\sum_{j=n_E+1}^{N_E} b_{E,j} p_{E,j}^{(2)} \right).$$

Recall that the basis functions $\{p_{E,j}^{(2)}\}$ have supports in \mathcal{K}_E^h . Thus, we have

$$\|p_h^{(B)} - \pi(p_h^{(B)})\|_Q^2 \lesssim h \|p_h^{(B)} - \pi(p_h^{(B)})\|_{L^2(\mathcal{E}_p)}^2$$

where $\|\cdot\|_{L^2(\mathcal{E}_p)}$ denotes the L^2 -norm defined on the set of coarse edges \mathcal{E}_p . Next, we define $w \in \widehat{V}_{\text{snap}}^{(2)}$ such that

$$[w \cdot n]|_E = -(p_h^{(B)} - \pi(p_h^{(B)}))|_E = \sum_{j=n_E+1}^{N_E} -b_{E,j} p_{E,j}^{(2)} \quad (56)$$

for all $E \in \mathcal{E}_p^0$, where $\widehat{V}_{\text{snap}}^{(2)}$ is the union of all $\widehat{V}_{E,\text{snap}}^{(2)}$, which is obtained by decoupling the continuity of normal components of basis functions in $V_{E,\text{snap}}^{(2)}$ on the edges in \mathcal{E}_p^0 . The condition (56) can be easily obtained by defining w as

$$w = \sum_{j=n_E+1}^{N_E} -b_{E,j} \phi_{E,j}^{(2)}$$

on one of the two coarse elements, denoted by K_E , having the edge E and as zero on the other coarse element, for every $E \in \mathcal{E}_p^0$. Using (14) and (5), we get

$$\sum_{E \in \mathcal{E}_p^0} \int_E p_h^{(B)} \sum_{j=n_E+1}^{N_E} b_{E,j} p_{E,j}^{(2)} = \int_{\Omega} \kappa \frac{\partial v_h}{\partial t} \cdot w. \quad (57)$$

In addition, by the orthogonality of eigenfunctions, it is easy to see that

$$\|p_h^{(B)} - \pi(p_h^{(B)})\|_{L^2(\mathcal{E}_p)}^2 = \sum_{E \in \mathcal{E}_p^0} b_{E,j}^2 \sum_{j=n_E+1}^{N_E} \int_E (p_{E,j}^{(2)})^2 = \sum_{E \in \mathcal{E}_p^0} \int_E p_h^{(B)} \sum_{j=n_E+1}^{N_E} b_{E,j} p_{E,j}^{(2)}. \quad (58)$$

On the other hand, by the Cauchy-Schwarz inequality, we have

$$\int_{\Omega} \kappa \frac{\partial v_h}{\partial t} \cdot w \lesssim \left\| \frac{\partial v_h}{\partial t} \right\|_V \|w\|_V$$

and by the definition of w , we have

$$\|w\|_V^2 \leq \sum_{E \in \mathcal{E}_p^0} \sum_{j=n_E+1}^{N_E} b_{E,j}^2 \int_{K_E} \kappa \phi_{E,j}^2 \leq \sum_{E \in \mathcal{E}_p^0} \sum_{j=n_E+1}^{N_E} b_{E,j}^2 \int_{\omega_E} \kappa \phi_{E,j}^2.$$

By the spectral problem (17),

$$\int_{\omega_E} \kappa \phi_{E,j}^2 = \frac{1}{\lambda_{E,j}} \int_E (\phi_{E,j} \cdot n)^2 = \frac{1}{\lambda_{E,j}} \int_E (p_{E,j}^{(2)})^2. \quad (59)$$

Combining (56), (57), (58) and (59), we obtain

$$\|p_h^{(B)} - \pi(p_h^{(B)})\|_{L^2(\mathcal{E}_p)}^2 \lesssim \left(\max_{E \in \mathcal{E}_p^0} \lambda_{E,n_E+1}^{-1} \right) \left\| \frac{\partial v_h}{\partial t} \right\|_V^2$$

This completes the proof. \square

Finally, we prove the following convergence theorem.

Theorem 5.5. Let (v_H, p_H) be the solution of the mixed GMsFEM (28)-(29), and let $\pi(v_h)$, $\pi(p_h^{(I)})$ and $\pi(p_h^{(B)})$ be the interpolants defined in (40). We have

$$\begin{aligned}
& \max_{0 \leq t \leq T} \left(\|\pi(v_h) - v_H\|_V^2 + \|\pi(p_h^{(I)}) + \pi(p_h^{(B)}) - p_H\|_Q^2 \right) \\
& \lesssim \left(\max_{E \in \mathcal{T}^H} \lambda_{E, n_E+1}^{-1} \right) \sum_{E \in \mathcal{E}^H} \int_0^T \int_E (\dot{v}_h \cdot n)^2 + h \left(\max_{E \in \mathcal{T}^H} \lambda_{E, n_E+1}^{-1} \right) \sum_{E \in \mathcal{E}^H} \int_0^T \int_E (\ddot{v}_h \cdot n)^2 \\
& + \left(\max_{K \in \mathcal{T}^H} \mu_{K, m_K+1}^{-1} \right) \int_0^T \left(\|\rho^{-1} \dot{f} - \dot{p}_h\|_Q^2 + \|\ddot{v}_h\|_V^2 \right).
\end{aligned} \tag{60}$$

Proof. The required bound is the consequence of (50), Theorem 5.3 and Theorem 5.4. \square

We remark that upper bounds for $\|v_h - v_H\|_V$ and $\|p_h - p_H\|_Q$ follow easily from the above theorem.

6 Numerical Results

In this section, we present some numerical results to show the performance of our method. In our simulations, the computational domain $\Omega = [0, 1]^2$, $\rho = 1$ and the source term f is chosen as the Ricker wavelet

$$f(x, t) = g(x)(t - 2/f_0)e^{-\pi^2 f_0^2 (t - 2/f_0)^2}, \quad g(x) = \delta^{-2} e^{-(x-0.5)^2 + (y-0.5)^2 / \delta^2}$$

where f_0 is the central frequency and $\delta = 2h$ measures the size of the support of the source. We assume that the initial conditions are zero. In the first two examples, we will consider the performance of our mixed GMsFEM for the propagation of the above point source with two types of heterogeneities and with the homogeneous Dirichlet boundary condition. In our third example, we will apply the perfectly matched layer (PML) [3] to simulate wave propagation in an unbounded domain containing a heterogeneous medium.

6.1 A layered stochastic coefficient

In our first example, we consider κ^{-1} as a layered stochastic medium shown in Figure 3. We will first construct the initial mesh \mathcal{T}_0^H for the domain $\Omega = [0, 1] \times [0, 1]$. To do so, we first define a uniform triangular coarse mesh on Ω with mesh size $H = 1/8$. This triangular mesh is obtained by first dividing the domain into uniform squares and then dividing each square into two triangles using the diagonal. This process gives the initial mesh \mathcal{T}_0^H . The required coarse mesh \mathcal{T}^H is then obtained by the process described in Section 2. Next, to construct the fine mesh \mathcal{T}^h , each coarse triangular element in \mathcal{T}^H is sub-divided into a union of uniform triangular fine mesh blocks with mesh size $h = 1/64$ in the standard way. Notice that, each coarse triangular element in \mathcal{T}^H is divided into 64 fine triangles. We choose the source frequency $f_0 = 20$, and compute the solution at the time $T = 0.2$. The reference solution at time $T = 0.2$ is shown in Figure 4. We apply our mixed GMsFEM (28)-(29) for this problem with various choices of number of basis functions. We will call the basis functions resulting from the first and the second basis sets the *boundary basis* and the basis functions resulting from the third basis set the *interior basis*. In Table 1, we present the relative errors of the pressure p in terms of the Q norm for various choices of number of basis functions. In particular, we use 3 to 6 basis functions per coarse edge for boundary basis and use 4 to 16 basis functions per coarse element for interior basis. We observe excellent performance of our method. For reference, the fine grid solver has 24576 unknowns for the pressure p and 28928 unknowns for the velocity v . From Table 1, we see that a very small dimensional approximation space can give an error below 5%. For instance, with the use of 4 boundary basis functions per coarse edge and the use of 12 interior basis functions per coarse element, the dimensions of the spaces V_H and Q_H are 7680 and 5312 respectively. We remark that we observe a similar accuracy behavior for the velocity, and we therefore skip those results in the paper.

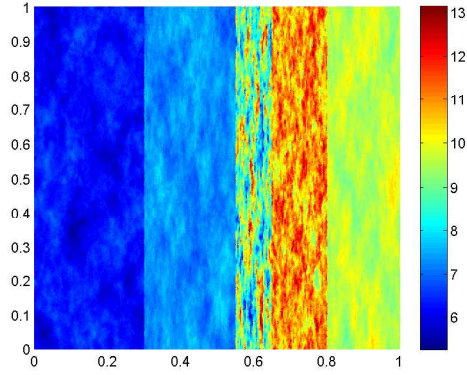


Figure 3: A stochastic coefficient for the first example.

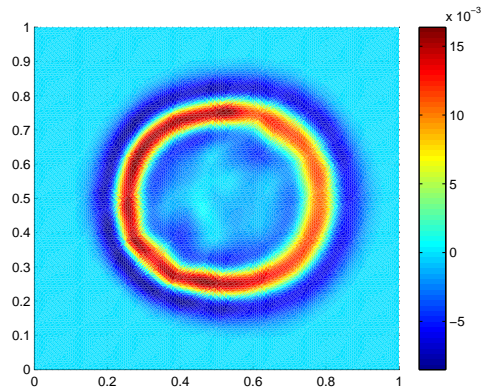


Figure 4: The reference solution for the first example.

# boundary basis \ # interior basis	4	8	12	16
3	13.22%	8.75%	7.84%	7.63%
4	12.76%	5.76%	3.65%	2.95%
5	12.97%	5.64%	3.31%	2.47%
6	13.01%	5.65%	3.31%	2.46%

Table 1: Convergence history for various choices of number of basis functions for the first example.

6.2 The Marmousi model

In our second example, we consider κ^{-1} as a part of the Marmousi model shown in Figure 5. We assume that the domain $\Omega = [0, 1] \times [0, 1]$ is partitioned as the first example with coarse mesh size $H = 1/16$ and the fine mesh size $h = 1/256$. We take the source frequency $f_0 = 20$, and compute the solution at the time $T = 0.2$. The reference solution and the multiscale solution using 6 boundary basis functions per coarse edge and 12 interior basis functions per coarse element at the time $T = 0.2$ are shown in Figure 6, and we observe very good agreement. In Table 2, we present the relative errors of the pressure p in terms of the Q norm for various choices of number of basis functions. In particular, we use 3 to 6 basis functions per coarse edge for boundary basis and use 4 to 12 basis functions per coarse element for interior basis. We again observe excellent performance of our method. For reference, the fine grid solver has 98304 unknowns for the pressure

p and 135296 unknowns for the velocity v . From Table 1, we see that with the use of 6 boundary basis functions per coarse edge and the use of 12 interior basis functions per coarse element, the relative error for the pressure is 8.59%, and the dimensions of the spaces V_H and Q_H are 36864 and 22848 respectively.

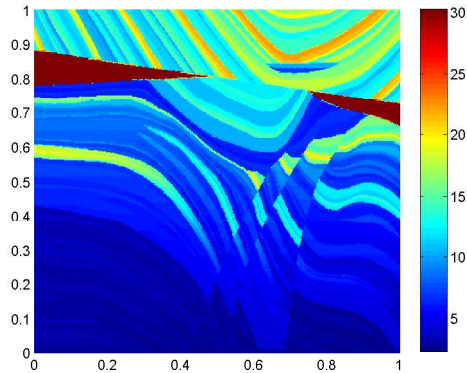


Figure 5: The Marmousi model for the second example.

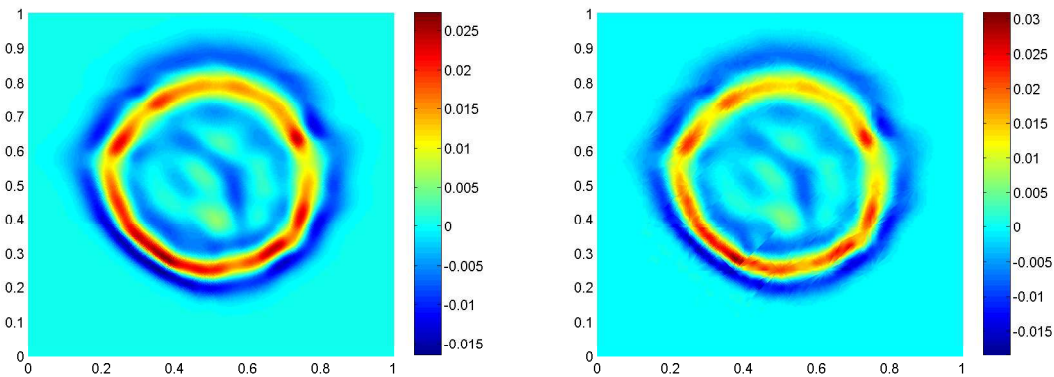


Figure 6: Left: The reference solution for the second example with $f_0 = 20$. Right: The corresponding multiscale solution for the second example using 6 boundary basis functions per coarse edge and 12 interior basis functions per coarse element.

# boundary basis \ #interior basis	4	8	12
3	46.66%	45.64%	46.02%
4	38.11%	23.83%	23.39%
5	40.35%	13.66%	10.84%
6	41.58%	12.91%	8.59%

Table 2: Convergence history for various choices of number of basis functions for the second example with $f_0 = 20$.

To further test the performance of our method, we take a higher frequency source term with $f_0 = 50$ and compute the solution at $T = 0.16$. The reference solution and the corresponding multiscale solution with 8 boundary basis functions per coarse edge and 20 interior basis functions per coarse element are shown in

Figure 7, and we observe very good agreement. In addition, the relative errors of the pressure p in terms of the Q norm for various choices of number of basis functions are presented in Table 3. In particular, we use 2 to 8 basis functions per coarse edge for boundary basis and use 4 to 20 basis functions per coarse element for interior basis. From this table, we observe excellent performance of our method.

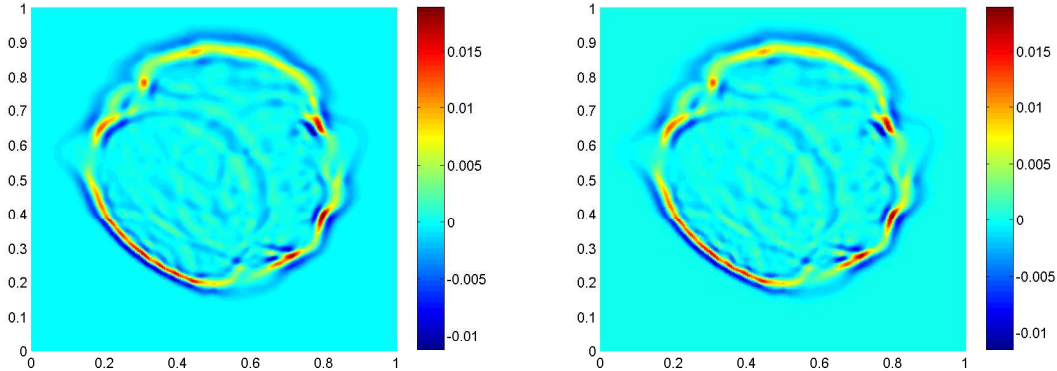


Figure 7: Left: The reference solution for the second example with $f_0 = 50$. Right: The corresponding multiscale solution for the second example using 8 boundary basis functions per coarse edge and 20 interior basis functions per coarse element.

# boundary basis \ #interior basis	4	8	12	16	20
2	125.75%	128.19%	129.09%	129.29%	129.37%
4	91.55%	58.00%	61.29%	62.87%	63.48%
6	100.46%	36.11%	18.65%	16.95%	17.04%
8	101.04%	40.67%	16.95%	9.41%	6.92%

Table 3: Convergence history for various choices of number of basis functions for the second example with $f_0 = 50$.

6.3 The Marmousi model with PML

In the third example, we present an application of our method with the use of PML. We assume that the computational domain $\Omega = [0, 1]^2$ and the medium is the part of the Marmousi model shown in Figure 5. We take the source with $f_0 = 20$. The coarse and fine mesh sizes for the computational domain Ω are $H = 1/8$ and $h = 1/64$ respectively. To absorb the outgoing waves, we use a PML with a width of 10 fine grid blocks. We apply our mixed GMsFEM within the computational domain Ω and the standard fine-grid method (3)-(4) within the artificial layer. In Figure 8, we present the multiscale scale solutions at different times T . We see that the PML is able to absorb the outgoing waves without much artificial reflection.

7 Conclusion

We develop and analyze a mixed GMsFEM for wave propagation in highly heterogeneous media. The method is based on a mixed Galerkin global solver, and some local multiscale basis functions for both the pressure and the velocity. The multiscale basis functions are obtained by solving local spectral problems defined in some snapshot spaces. The spectral problems give a natural ordering of the basis functions, which can be added to the approximation space to give a spectral convergence. By using a staggered coarse mesh and a carefully

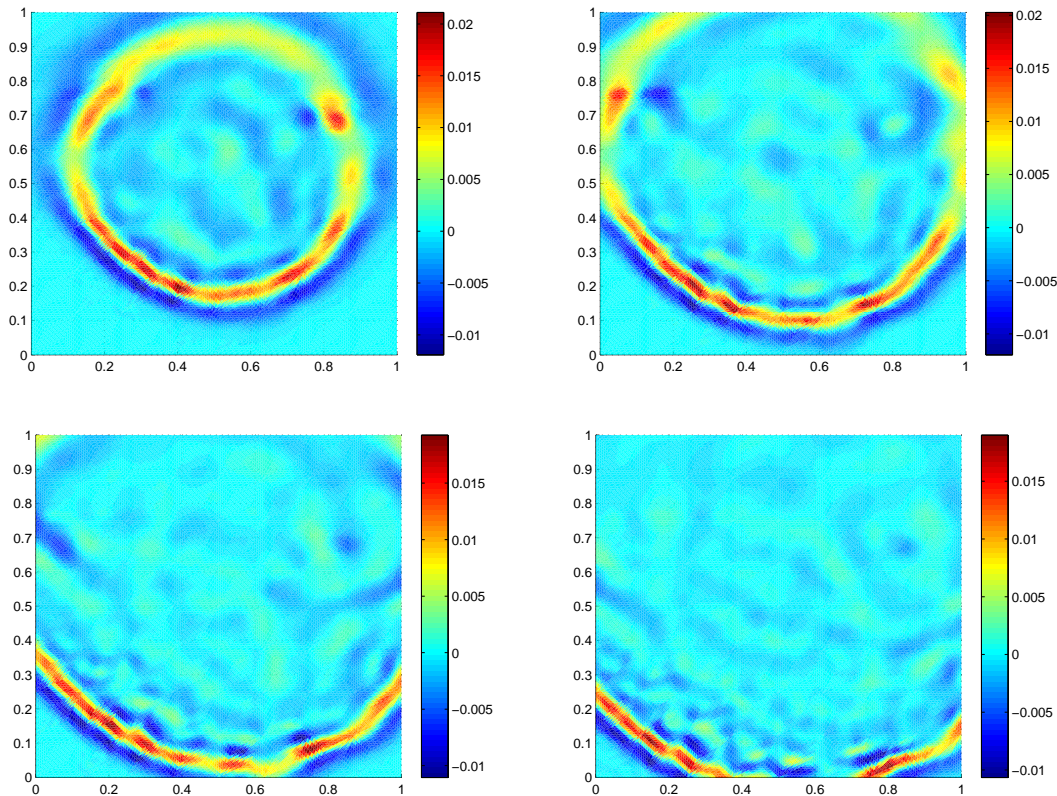


Figure 8: The multiscale solution at different times T for the third example. Top-Left: $T = 0.24$, Top-Right: $T = 0.28$, Bottom-Left: $T = 0.32$, Bottom-Right: $T = 0.36$.

designed pair of multiscale basis spaces with staggered continuity, our method is energy conserving and has block diagonal mass matrix. Numerical results show excellent performance for our proposed approach.

References

- [1] Assyr Abdulle and Marcus J Grote. Finite element heterogeneous multiscale method for the wave equation. *Multiscale Modeling & Simulation*, 9(2):766–792, 2011.
- [2] Assyr Abdulle, Marcus J Grote, and Christian Stohrer. Finite element heterogeneous multiscale method for the wave equation: Long-time effects. *Multiscale Modeling & Simulation*, 12(3):1230–1257, 2014.
- [3] Jean-Pierre Berenger. A perfectly matched layer for the absorption of electromagnetic waves. *Journal of computational physics*, 114(2):185–200, 1994.
- [4] H. Chan, E. Chung, and G. Cohen. Stability and dispersion analysis of staggered discontinuous Galerkin method for wave propagation. *Int. J. Numer. Anal. Model.*, 10:233–256, 2013.
- [5] E. Chung, Y. Efendiev, and R. Gibson. An energy-conserving discontinuous multiscale finite element method for the wave equation in heterogeneous media. *Advances in Adaptive Data Analysis*, 3:251–268, 2011.

- [6] E. Chung and B. Engquist. Optimal discontinuous Galerkin methods for wave propagation. *SIAM J. Numer. Anal.*, 44:2131–2158, 2006.
- [7] E. Chung and B. Engquist. Optimal discontinuous Galerkin methods for the acoustic wave equation in higher dimensions. *SIAM J. Numer. Anal.*, 47:3820–3848, 2009.
- [8] E. Chung and P. Ciarlet Jr. A staggered discontinuous Galerkin method for wave propagation in media with dielectrics and meta-materials. *J. Comput. Appl. Math.*, 239:189–207, 2013.
- [9] E. Chung, P. Ciarlet Jr., and T. Yu. Convergence and superconvergence of staggered discontinuous Galerkin methods for the three-dimensional Maxwell’s equations on Cartesian grids. *J. Comput. Phys.*, 235:14–31, 2013.
- [10] E. Chung, H. Kim, and O. Widlund. Two-level overlapping Schwarz algorithms for a staggered discontinuous Galerkin method. *SIAM J. Numer. Anal.*, 51:47–67, 2013.
- [11] E. Chung and C. Lee. A staggered discontinuous Galerkin method for the convection-diffusion equation. *J. Numer. Math.*, 20:1–31, 2012.
- [12] E. Chung and C. Lee. A staggered discontinuous Galerkin method for the curl-curl operator. *IMA J. Numer. Anal.*, 32:1241–1265, 2012.
- [13] Eric T Chung, Yalchin Efendiev, and Chak Shing Lee. Mixed generalized multiscale finite element methods and applications. *Multiscale Modeling & Simulation*, 13(1):338–366, 2015.
- [14] Eric T Chung, Yalchin Efendiev, and Wing Tat Leung. Generalized multiscale finite element methods for wave propagation in heterogeneous media. *Multiscale Modeling & Simulation*, 12(4):1691–1721, 2014.
- [15] Eric T Chung, Yalchin Efendiev, and Wing Tat Leung. Residual-driven online generalized multiscale finite element methods. *arXiv preprint arXiv:1501.04565*, 2015.
- [16] Eric T Chung, Yalchin Efendiev, and Guanglian Li. An adaptive gmsfem for high-contrast flow problems. *Journal of Computational Physics*, 273:54–76, 2014.
- [17] Jonas D. De Basabe and Mrinal K. Sen. New developments in the finite-element method for seismic modeling. *The Leading Edge*, 28(5):562–567, 2009.
- [18] Florence Delprat-Jannaud and Patrick Lailly. Wave propagation in heterogeneous media: Effects of fine-scale heterogeneity. *Geophysics*, 73(3):T37–T49, 2008.
- [19] Y. Efendiev, J. Galvis, and T. Hou. Generalized multiscale finite element method. *Journal of Computational Physics*, 251:116–135, 2012.
- [20] Yalchin Efendiev and Thomas Y Hou. *Multiscale finite element methods: theory and applications*, volume 4. Springer Science & Business Media, 2009.
- [21] Bjorn Engquist, Henrik Holst, and Olof Runborg. Multi-scale methods for wave propagation in heterogeneous media. *arXiv preprint arXiv:0911.2638*, 2009.
- [22] Björn Engquist, Henrik Holst, and Olof Runborg. Multiscale methods for wave propagation in heterogeneous media over long time. In *Numerical analysis of multiscale computations*, pages 167–186. Springer, 2012.
- [23] Jacob Fish and Wen Chen. Space–time multiscale model for wave propagation in heterogeneous media. *Computer Methods in applied mechanics and engineering*, 193(45):4837–4856, 2004.
- [24] Kai Gao, Eric T Chung, Richard L Gibson Jr, Shubin Fu, and Yalchin Efendiev. A numerical homogenization method for heterogeneous, anisotropic elastic media based on multiscale theory. *Geophysics*, 80(4):D385–D401, 2015.

- [25] Kai Gao, Shubin Fu, Richard L Gibson, Eric T Chung, and Yalchin Efendiev. Generalized multi-scale finite-element method (gmsfem) for elastic wave propagation in heterogeneous, anisotropic media. *Journal of Computational Physics*, 295:161–188, 2015.
- [26] R. Gibson, K. Gao, E. Chung, and Y. Efendiev. Multiscale modeling of acoustic wave propagation in two-dimensional media. *To appear in Geophysics*.
- [27] Verena Hermann, Martin Käser, and Cristóbal E. Castro. Non-conforming hybrid meshes for efficient 2-D wave propagation using the discontinuous Galerkin method. *Geophysical Journal International*, 184(2):746–758, 2011.
- [28] Lijian Jiang, Yalchin Efendiev, and Victor Ginting. Analysis of global multiscale finite element methods for wave equations with continuum spatial scales. *Applied Numerical Mathematics*, 60(8):862–876, 2010.
- [29] Martin Käser, Christian Pelties, Cristobal E. Castro, Hugues Djikpesse, and Michael Prange. Wavefield modeling in exploration seismology using the discontinuous Galerkin finite-element method on HPC infrastructure. *The Leading Edge*, 29(1):76–85, 2010.
- [30] Dimitri Komatitsch, Dominik Góddeke, Gordon Erlebacher, and David Michéa. Modeling the propagation of elastic waves using spectral elements on a cluster of 192 GPUs. *Computer Science - Research and Development*, 25:75–82, 2010. 10.1007/s00450-010-0109-1.
- [31] Dimitri Komatitsch and Jeroen Tromp. Introduction to the spectral element method for three-dimensional seismic wave propagation. *Geophysical Journal International*, 139(3):806–822, 1999.
- [32] Dimitri Komatitsch and Jeroen Tromp. Spectral-element simulations of global seismic wave propagation—I. Validation. *Geophysical Journal International*, 149(2):390–412, 2002.
- [33] Oksana Korostyshevskaya and Susan E Minkoff. A matrix analysis of operator-based upscaling for the wave equation. *SIAM Journal on Numerical Analysis*, 44(2):586–612, 2006.
- [34] B. Lombard, J. Piraux, C. Gélis, and J. Virieux. Free and smooth boundaries in 2-D finite-difference schemes for transient elastic waves. *Geophysical Journal International*, 172(1):252–261, 2008.
- [35] Y. J. Masson and S. R. Pride. Finite-difference modeling of Biot’s poroelastic equations across all frequencies. *Geophysics*, 75(2):N33–N41, 2010.
- [36] Peter Moczo, Jozef Kristek, Martin Galis, Emmanuel Chaljub, and Vincent Etienne. 3-D finite-difference, finite-element, discontinuous-Galerkin and spectral-element schemes analysed for their accuracy with respect to p-wave to s-wave speed ratio. *Geophysical Journal International*, 187(3):1645–1667, 2011.
- [37] Christina Morency, Yang Luo, and Jeroen Tromp. Acoustic, elastic and poroelastic simulations of CO₂ sequestration crosswell monitoring based on spectral-element and adjoint methods. *Geophysical Journal International*, pages no–no, 2011.
- [38] Houman Owhadi and Lei Zhang. Numerical homogenization of the acoustic wave equations with a continuum of scales. *Computer Methods in Applied Mechanics and Engineering*, 198(3):397–406, 2008.
- [39] C. Pelties, M. Käser, V. Hermann, and C. E. Castro. Regular versus irregular meshing for complicated models and their effect on synthetic seismograms. *Geophysical Journal International*, pages no–no, 2010.
- [40] Erik H. Saenger, Radim Ciz, Oliver S. Krüger, Stefan M. Schmalholz, Boris Gurevich, and Serge A. Shapiro. Finite-difference modeling of wave propagation on microscale: A snapshot of the work in progress. *Geophysics*, 72(5):SM293–SM300, 2007.

- [41] William Symes, Igor S. Terentyev, and Tetyana Vdovina. Getting it right without knowing the answer: Quality control in a large seismic modeling project. *SEG Technical Program Expanded Abstracts*, 28(1):2602–2606, 2009.
- [42] Tetyana Vdovina, Susan E Minkoff, and Oksana Korostyshevskaya. Operator upscaling for the acoustic wave equation. *Multiscale Modeling & Simulation*, 4(4):1305–1338, 2005.
- [43] Jean Virieux. SH-wave propagation in heterogeneous media: Velocity-stress finite-difference method. *Geophysics*, 49(11):1933–1942, 1984.
- [44] Jean Virieux. P-SV wave propagation in heterogeneous media: Velocity-stress finite-difference method. *Geophysics*, 51(4):889–901, 1986.
- [45] E Weinan, Bjorn Engquist, Xiantao Li, Weiqing Ren, and Eric Vanden-Eijnden. Heterogeneous multi-scale methods: a review. *Commun. Comput. Phys*, 2(3):367–450, 2007.
- [46] W. Zhang, L. Tong, and E. Chung. Exact nonreflecting boundary conditions for three dimensional poroelastic wave equations. *Comm. Math. Sci.*, To appear.
- [47] W. Zhang, L. Tong, and E. Chung. A new high accuracy locally one-dimensional scheme for the wave equation. *J. Comput. Appl. Math.*, 236:1343–1353, 2011.
- [48] W. Zhang, L. Tong, and E. Chung. Efficient simulation of wave propagation with implicit finite difference schemes. *Numer. Math. Theor. Meth. Appl.*, 5:205–228, 2012.